

# Machine Learning Approaches for Automated Stroke Detection, Segmentation, and Classification in Microwave Brain Imaging Systems

Majid Roohi<sup>1</sup>, Jalil Mazloum<sup>2, \*</sup>, Mohammad-Ali Pourmina<sup>1</sup>, and Behbod Ghalamkari<sup>1</sup>

**Abstract**—In this paper, an intracranial hemorrhage stroke detection and classification method using microwave imaging system (MIS) based on machine learning approaches is presented. To create a circular array-based MIS, sixteen elements of modified bow-tie antennas around a multilayer head phantom with a spherical target with radius of 1 cm as an intracranial hemorrhage target are simulated in CST simulator. To obtain satisfied radiation characteristics in the desired frequency band of 0.5–5 GHz a suitable matching medium is designed. Initially, in the processing section, a confocal image-reconstructing method based on delay-multiply-and-sum (DMAS) beam-forming algorithms is used. Then, reconstructed images are generated, which shows the applicability of the confocal method in detecting a spherical target in the range of 1 cm. Separating and categorizing targets is a challenging task due to the ambiguity in the extracted target from MIS. Thus, to distinguish between healthy and unhealthy brain tissues, a new compound machine learning technique, including filtering, edge-detection based segmentation, and applying K-Means and fuzzy clustering techniques, which reveal intracranial hemorrhage area from reconstructed images is adopted. Simulated results are presented to validate the proposed method effectiveness for precisely localizing and classifying bleeding targets.

## 1. INTRODUCTION

The objective of microwave imaging system (MIS) for human head imaging applications is to detect cancerous tumors, brain injuries that cause ischemic or hemorrhage strokes, and brain activity monitoring [1, 2]. There are several key factors in the imaging process, e.g., antenna dimension and its radiation characteristics, image reconstruction methods, and post-processing techniques [3–5]. Several imaging methods have been proposed to be utilized in medical imaging systems. These methods are generally categorized in two main branches known as quantitative and qualitative methods. Quantitative methods, such as the region of interest (ROI) tomography extract dielectric constant, are based on iterative methods. The images reconstructed by these methods have good spatial resolution at the cost of considerable computation time. On the other hand, qualitative methods, such as radar-based methods, are based on reflected signal delays and are considered as a real-time method. These are faster than the quantitative methods and thus more suitable for pre-hospital use.

A variety of methods have been proposed for reconstructing microwave images. However, in the post-processing part, which adopts machine learning methods to classify different stroke types, much research has not been done. On the other hand, there are many difficulties and challenges in classifying stroke types due to the type of images extracted from radar systems. Machine learning techniques applied to MIS have great potential in enabling segmentation, clustering, and classification cases [6–15].

---

*Received 4 August 2021, Accepted 3 November 2021, Scheduled 11 November 2021*

\* Corresponding author: Jalil Mazloum (jalil.mazloum@ssau.ac.ir).

<sup>1</sup> Department of Electrical and Computer Engineering, Science and Research Branch, Islamic Azad University (IAU), Tehran, Iran.

<sup>2</sup> Department of Electrical Engineering, Shahid Sattari Aeronautical University of Science and Technology, Tehran, Iran.

In [8], a neural network is combined with microwave imaging to learn the forward model for a complex data-acquisition system. In addition, Franceschini et al. proposed a radial basis function neural network to estimate the position and size of proliferated marrow inside bone tissue with microwave imaging [9]. Bevacqua et al. tried to take the benefit of a deep neural network to enhance the constructed images [10]. Their deep neural network was trained to take microwave images created using the back-projection method as an input and had a much-improved image of the network output. In fact, they tried to bypass the use of iterative techniques for solving the full nonlinear electromagnetic inverse problem. Also, utilizing deep learning techniques to improve 2D microwave imaging for breast imaging application has been investigated [11]. Researchers employing radar-based techniques have also investigated machine learning approaches to detect breast lesions [12]. In [13], a new classification approach is presented for the automatic diagnosis of reconstructed images based on microwave tomography, e.g., it can be applied to discriminate a cancerous tumor inside breast tissue. Microwave tomography systems work with reconstructed images created based on the medium dielectric properties. Other classification types are directly based on the signal feature disregarding the dielectric property's reconstruction. For instance, a new method for distinguishing intracervical hemorrhage (ICH) from ischemic stroke (IS) is presented in [14, 15].

In this paper, the advantages of using machine learning technique for localizing and detecting hemorrhage stroke in a precisely modeled full head phantom in compact multi-static imaging system are explored. In this context, a modified compact matched bow-tie antenna design with a matching balun in the feed-line is presented. By adopting these modified structures, the usable frequency of the proposed slot antenna is progressed from 0.5 GHz to 5 GHz. Then, 2D images are reconstructed based on the confocal image reconstruction algorithm. Because in a radar-based microwave imaging system, images are extracted from the return signals recorded by a reconstruction algorithm based on the display of energy concentrated at each focal point, there are many challenges in detecting location and related boundaries. There is a purpose to the image. From this point of view, this paper tries to simulate the image extracted from the simulation environment with real scenarios by the existing methods in image processing by adding parameters such as noise. Also, using intelligent segmentation and categorization methods, the boundaries of the main purpose of the image should be clearly defined. These techniques can be used to help to clearly decide the purpose of the target and its exact location. Due to the clustering importance to discernment of hemorrhage from IS after generating an image from the ROI, a novel combined post-processing method is applied. Thus, the detailed procedures like filtering, contrast enhancement, and edge detection are first applied. Then, the post-processing phase involves segmentation and applying K-Means and fuzzy clustering methods. The validity of the presented system and its target detection algorithm accuracy are verified by simulations. Results obtained by the proposed multi-static imaging system prove that the proposed machine learning approach based system has a good ability to locate and separate the intracranial hemorrhage strokes area inside a multi-layer head phantom.

## 2. THE PROPOSED MICROWAVE IMAGING SETUP AND ANTENNA CONFIGURATION DESIGN

The proposed simulated microwave head imaging schematic scenario with sixteen UWB bow-tie antennas is presented in Fig. 1. To realize this system, the precisely multi-layer human head phantom model is created in CST simulator [16]. In order to calibrate the coordination of imaging scenario, the head model with realistic shape and size as the human head is constructed (with dimensions  $x = 220$  mm and  $y = 170$  mm). The configuration of the antenna different positions around the head is shown in Fig. 1. As shown in Fig. 3, sixteen positions of the proposed setup encircle the head at equal distances 20 mm from the skull layer. The signals are collected by changing the antenna position in each 22.5 degrees. The head phantom contains all anatomical details of the human head, including all head layers, from the skin to white brain matter, for ease of modeling and imaging. All electrical characteristics of the utilized head phantom's materials are given in Table 1. In addition, as shown in Fig. 1(a), all sixteen proposed antennas encircle the head at an equal distance of 10 mm from the skin layer, and a hemorrhage stroke is located inside the head, as shown in Fig. 1.

It is well known that printed microstrip antennas have a variety of applications, especially

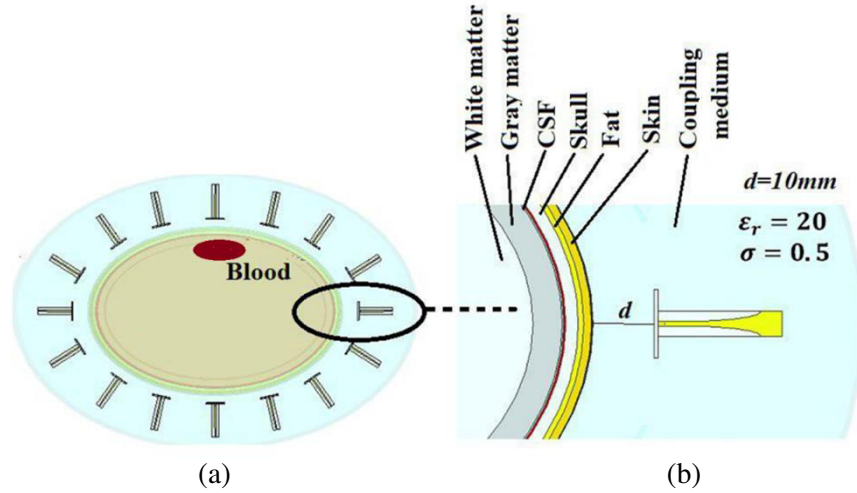


**Figure 1.** Multi-static UWB MIS schematic for haemorrhage stroke detection, (a) simulated head model with a hemorrhage stroke in CST medium, (b) multi layer structure of the designed head phantom and antenna’s positions.

**Table 1.** Electrical characteristics of the multi-layer brain phantom.

| Layer        | R (mm) | r (mm) | Depth (mm) |
|--------------|--------|--------|------------|
| Skin         | 120    | 80     | 2          |
| Fat          | 118    | 78     | 1.4        |
| Skull        | 116.6  | 76.6   | 4.1        |
| CSF          | 113.4  | 73.4   | 0.5        |
| Gray Matter  | 112.9  | 72.9   | 7          |
| White Matter | 105    | 65     | Inner part |
| Blood        | –      | 10     | 10         |

in biomedical applications, due to their simple structure and omnidirectional radiation pattern properties [17]. The proposed antenna structure is depicted in Fig. 2, which is a modified version of the antenna presented in [18]. The modifications in the antenna size allow for a higher frequency bandwidth to make it more applicable to the present study. The basic antenna structure consists of a radiating patch and a balun type feed line. The radiating patch is printed on a Rogers 5880 substrate with a dimension of  $22 \times 22 \text{ mm}^2$ , a thickness of 1.5 mm, a dielectric constant of 2.2, and a loss tangent of 0.001. The feeding line is printed on a Rogress 6010 substrate with a dimension of  $8 \times 40 \text{ mm}^2$ , a thickness of 1.27 mm, a dielectric constant of 10.2, and a loss tangent of 0.001. All antenna dimensions are specified in Table 2.

The antenna design in microwave brain imaging is quite different from free-space antenna design. It includes the antenna, matching medium, and a brain phantom. For this purpose, the antenna type is more important than the radiator part shape. Normally, simpler shapes yield better results, and microwave brain imaging is considered as an ultra-short range sensing method in lossy medium. Most papers studying this area have opted for simple antenna forms, e.g., bow-tie, dipole, and slot [1–5]. For the radiating section, one of the proposed structures in previous studies was modified [18], and then, in the presence of the phantom used in the present work, an appropriate matching medium was designed to obtain a suitable frequency bandwidth (BW) range for brain imaging applications (0.5–5 GHz). The reasons for choosing the proposed bow-tie antenna for this study are as follows:

- Constant phase center at different frequencies; To maintain a constant phase center is of utmost importance in image reconstruction algorithms. The antenna radiating patch center is the starting point

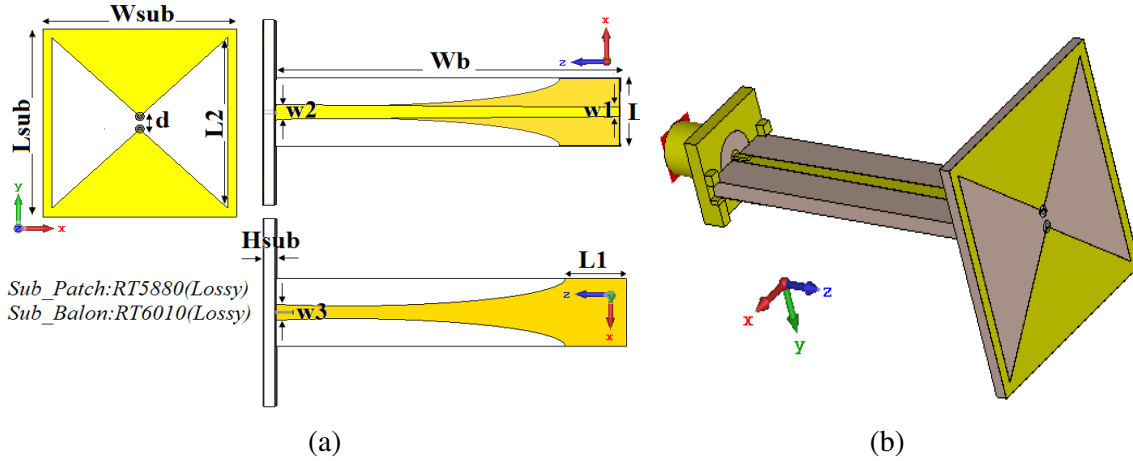


**Figure 2.** The proposed matched bowtie antenna with matching balun schematic, (a) patch and feeding line, and (b) side view [13].

**Table 2.** The proposed slot antenna dimensions.

| Parameter           | (mm) | Parameter   | (mm) |
|---------------------|------|-------------|------|
| <b>Wsub</b>         | 22   | <b>Lsub</b> | 22   |
| <b>Wb</b>           | 40   | <b>Lb</b>   | 8    |
| <b>W1</b>           | 1.1  | <b>W2</b>   | 1.75 |
| <b>W3</b>           | 1.84 | <b>L1</b>   | 7    |
| <b>L2</b>           | 20   | <b>Hsub</b> | 1.5  |
| <b>Hsub (Balun)</b> | 1.27 | <b>D</b>    | 1.5  |

location of all propagating waves at different frequencies, and reflected signals can be calibrated very easily.

- High-fidelity factor; Only by modifying the matching medium thickness and the distance between antenna and brain phantoms, the propagating wave front inside brain will be planar.

- It is very easy to use the vertical feed line, and it is suitable for embedding in hemisphere container.

The main challenge in antenna and wave-propagation section is designing a suitable matching medium. It is possible to decrease the antenna and head phantom mismatch effects by shielding the antennas in the matching medium [1]. To ensure electrical matching between the antennas and ROI under test, a coupling medium is designed based on the parametric sweep of its electrical characteristics. The calculated electrical characteristics of the coupling medium are  $\epsilon_r = 20$  and  $\sigma = 0.5 \text{ S/m}$ . Six samples of simulated reflection characteristics of the proposed antenna at different positions inside the designed matching medium are illustrated in Fig. 3. It can be seen that by choosing an appropriate matching medium permittivity and conductivity all sixteen antennas radiate from 0.5 to 5 GHz.

To illustrate the applicability of the proposed MIS for hemorrhage stroke detection, the confocal imaging algorithm is performed, and the results are analyzed and discussed. It is obvious that detecting hemorrhage stroke from head phantom is an emergency diagnostic case and needs to be considered as real-time data acquisition. All reflected signals obtained from the simulations are stored to reconstruct the images in MATLAB. Delays must be compensated for the integration of coherent signals, because the signals which are reflected in the multi-static delays have different path lengths. Therefore, an initial calibration considering antenna position delays has to be done. Thus, the phase shifting among all antennas have to be determined. This time delay is equal to the direct distance between the transmitter and receiver divided by the wave velocity in the coupling medium [19]. Then, the hemorrhage stroke location is extracted from the reflected signals. As this point is identified, all of the values are set as

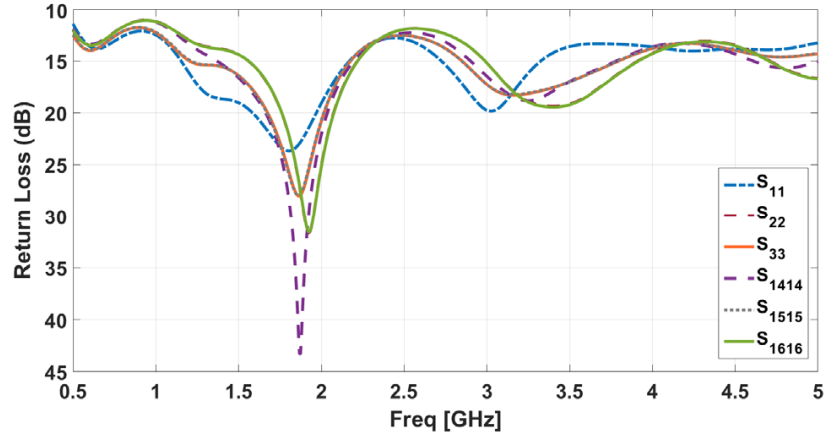


**Figure 3.** Six samples of the simulated return loss characteristics of the proposed antennas inside the proposed matching medium.

zero before the delays are calculated.

A focused beamforming algorithm, such as confocal focusing algorithm, is needed to reconstruct an image. Focusing algorithms are used to synchronize the signals collected during the data acquisition phase with respect to each brain focal point. In radar based modality, focusing algorithms include Delay and Sum (DAS), Delay-Multiply and Sum (DMAS), Improved Delay-And Sum (IDAS), Coherence Factor Based Delay-And-Sum (CFDAS), Channel Ranked Delay-And-Sum (CRDAS), Microwave Imaging via Space-Time (MIST), Multiple Signal Classification (MUSIC), Weighted Capon Beamforming (WCB), Robust Weighted Capon Beamforming (RWCB), Generalized Likelihood Ratio Test (GLRT), etc. [20–23]. All these focusing algorithms face performance degradation when being applied in brain situations. In addition, it is noted from various clinical trials that the average dielectric properties of brain tissues can vary substantially with geometry and density. This variation can impact both the image quality and sensitivity of imaging. In 2020, Benny et al. demonstrated the effectiveness of adopting parameter search algorithms to improve sensitivity of permittivity estimation techniques [21]. As a preliminary step, experimental phantoms (made of tissue mimicking materials) were imaged, and reconstruction performances of DAS, IDAS, DMAS, CFDAS, CRDAS, and RWCB were compared. Signal to Clutter Ratio (SCR), Signal to Mean Ratio (SMR), and localization error were selected as the comparison metric. DMAS was the only algorithm that significantly improved the image quality in terms of both SMR and SCR while keeping localization error within prescribed limits [23]. In 2018, these six algorithms were compared using actual clinical data [22]. The basic DAS algorithm was noted to be able to detect most malignancies, but the clutter level was significantly high. IDAS and CFDAS reported the highest SMR and hence reduced clutter levels; however, the responses often did not correspond to the actual lesion locations from clinical reports. CR-DAS and RCB performed poorly across all patients. DMAS showed the second highest SMR with an improvement of 44% in comparison to DAS and comparable clutter suppression to IDAS. DMAS also ranked the best in terms of localization of growths. The above-mentioned comparison studies were carried out without considering the inter-patient variations in breast dielectric properties. From the results reported by various research teams who compared the various focusing algorithms in radar imaging, DMAS is noted to have the most balanced performance and may be suggested as a suitable choice for future research efforts in this domain [24]. Then, the focal points are identified to calculate reflected signal energy patterns at these points, which is done by coherence signal integration for multi-static imaging algorithm. Regarding pulse-width and ROI dimension, 320 focal points are considered inside the ROI.

In the confocal image reconstruction method, the picture pixel intensity (brightness) at the  $n$ th range cell and direction  $\theta$  is represented by  $F_i(n)$ , given by the following relation:

$$F_i(n) = \sum_{n=1}^N f_i \cdot X_i(n) \cdot e^{j\phi_i} \quad (1)$$

A spherical wave front is assumed for the propagated wave inside the brain medium. In Eq. (1),  $X_i(n)$  is the complex value of the received signal from antenna, and  $N$  is the total number of receiving antennas. Further, to consider the medium effects, phantom mediums' attenuations, and propagation losses,  $f_i$  was added as weighting parameters. To compensate phase difference due to distinct traveling paths, the phase component  $\phi_i$  is utilized [24].

In this study, to create the image with increased target detection accuracy, the confocal image reconstruction algorithm based on an improved beamformer DMAS has been used. Similar to DAS, the DMAS works based on coherently energy integration by shifting the reflected signals in time-domain to make them coherent, then by summing the results the energy in focal points can be calculated. In the present study, the value of 36 for effective permittivity in the proposed multi-layer structure is calculated as the optimal path loss in reflected signals. Based on DAS beamforming method, for applying the confocal image reconstruction algorithm in the case of having  $M$  antennas and by considering  $S_n$  as the  $i$ th return signal to  $n$ th antenna, the energy in each focal point position  $r = [x; y; z]$  can be denoted as:

$$I(r) = \int_0^{T_w} \left[ \sum_{i=1}^M S_n(t - \tau_i(r)) \right]^2 dt \quad (2)$$

where  $\tau_i(r) = (2d_i(r))/(\nu T_s)$  is indicated as the  $i$ th discrete time-delay. In this case,  $d_i(r) = |r - r_i|$  demonstrates the discrete time-distance from the  $i$ th transmitting antenna  $r_n$  to the focal point  $r$ ;  $\nu$  indicates the average propagated wave velocity in the brain medium;  $T_w$  is the window length; and  $T_s$  is the sampling interval. In a multistatic system  $M^2$  signals can be recorded. However due to reciprocity, only  $M(M - 1)/2$  signals are required for the energy profile calculation. In the DMAS, unlike DAS, the multiplication of time-shifted signals are added together, and then in order to calculate the energy at a focal point the products are summed. The energy related to the focal point  $r = [x; y; z]$  within the brain medium is defined as:

$$I(r) = \int_0^{T_w} \left[ \sum_{i=1}^{M-1} \sum_{j=n+1}^M S_n(t - \tau_i(r)) S_j(t - \tau_j(r)) \right]^2 dt \quad (3)$$

where  $M$  indicates the number of antennas in the multi-static imaging scenario.

Through processing raw data, the 2D reconstructed image using the differential imaging scenario by subtracting a healthy brain image from the brain with stroke is shown in Fig. 4. As mentioned earlier in conventional confocal, DMAS beamformer is used. As illustrated in Fig. 4, the reconstructed image has a good resolution and contrast.

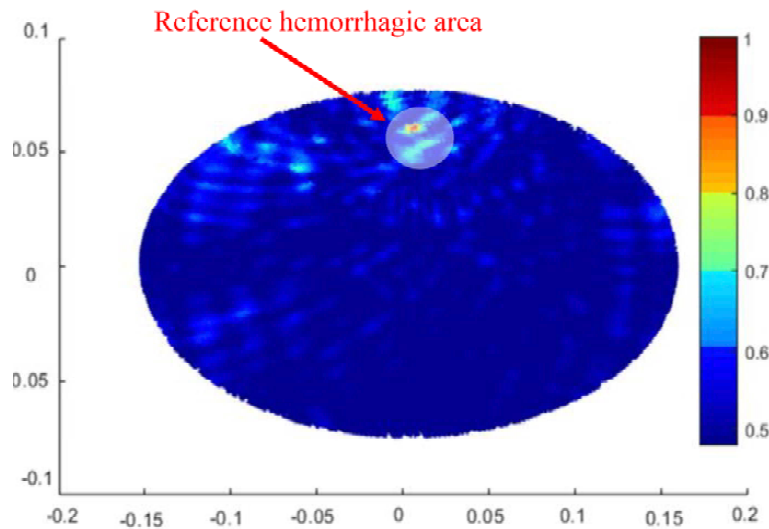


**Figure 4.** Reconstructed image from confocal image reconstruction method with DMAS beamforming.

### 3. PROPOSED POST-PROCESSING METHOD FOR SEGMENTATION AND CLASSIFICATION

After applying confocal image reconstruction algorithm as the processing section to separate the hemorrhage target from the brain medium, a new approach for automatic classification of the reconstructed images as healthy or unhealthy tissue using segmentation and classification algorithm is proposed. Fig. 5 shows the proposed stroke segmentation and classification method flowchart. The reconstructed image from the pre-processing and processing sections is used as input for the proposed post-processing algorithm.

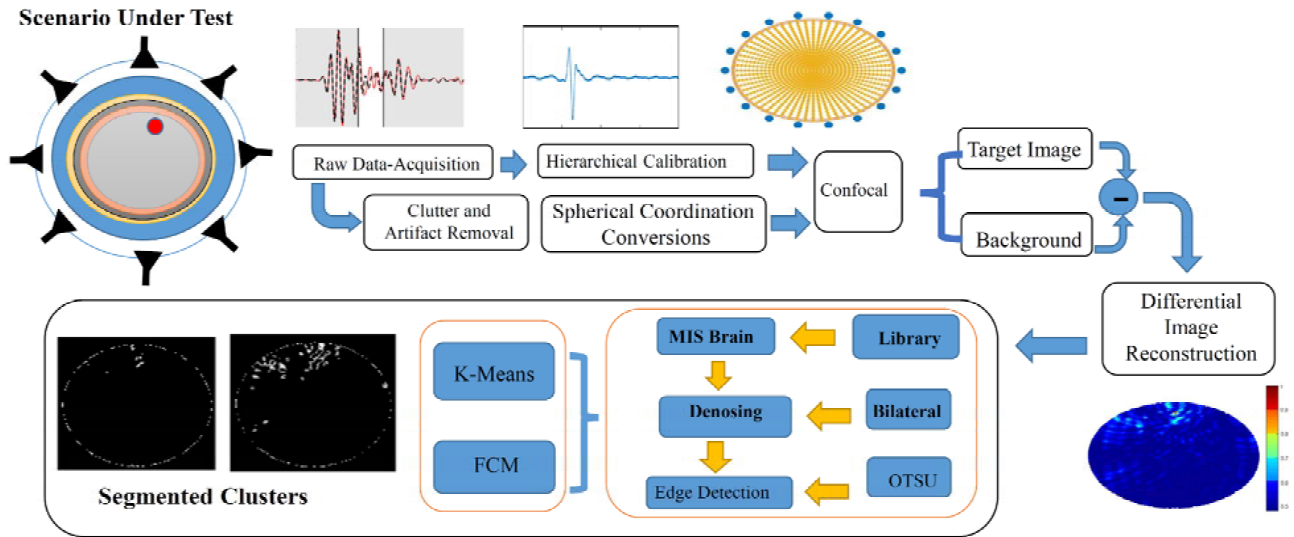


**Figure 5.** Proposed algorithm flowchart for stroke detection, classification, and segmentation (including each stage’s outcome).

The post-processing section is implemented in MATLAB. Segmentation is done based on image pixel value characteristics. The first step of this section is adding noise and employing denoising to demonstrate the proposed algorithm robustness for unexpected real-world issues. In addition, adding noise and applying noise removal methods also increase the efficiency of the algorithm in scenarios based on images extracted from real samples. For noise removal from the noisy image, normal shrink denoising algorithm is used. Then, the bilateral filter algorithm is applied to the output obtained image after de-noising for edge preservation. Fig. 6 shows image initialization process with a noisy image and the denoising section using normal shrink and also bilateral denoising filters effect on edge preservation [25].

The next step applied on the edge preserved image is the edge-based segmentation process. Here, a Kirsch operator using a  $3 \times 3$  mask was implemented [26]. In addition, Sobel operator using a  $3 \times 3$  mask was implemented. Then, an advanced Sobel operator using a  $5 \times 5$  mask was adopted. Fig. 7 shows the segmented images of the Kirsch operator using a  $3 \times 3$  mask, Sobel operator using a  $5 \times 5$  mask, and OTSU method to perform automatic image thresholding. As seen in Fig. 7(c), target regions are very well distinguished from the normal tissue regions by processing edge segmentation using the OTSU segmentation. The main challenge with microwave images for separating targets is that the energies accumulated from the antennas vary depending on the reflections in the simulation environment. The concentrated energy has different values at each focal point. So, a threshold is assumed for the OTSU. In image processing, Otsu’s method is used to perform automatic image thresholding [27]. In the simplest form, the algorithm returns a single intensity threshold that separates pixels into two classes, foreground and background. This threshold is determined by minimizing intra-class intensity variance, or equivalently, by maximizing inter-class variance. Otsu’s method is a one-dimensional discrete analog of Fisher’s Discriminant Analysis, is related to Jenks optimization method, and is equivalent to a globally

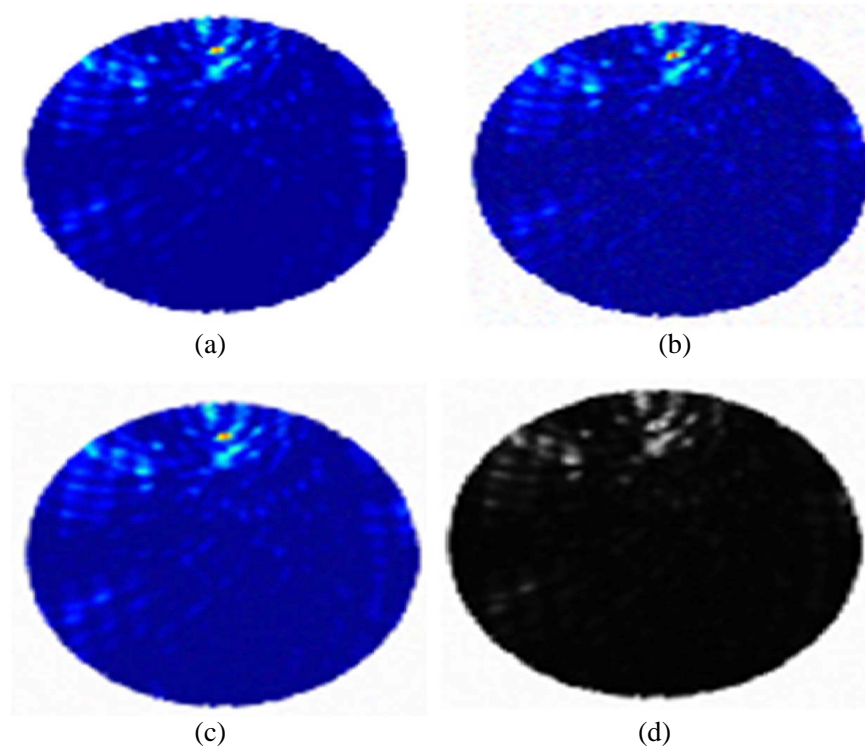


**Figure 6.** Image initialization process (a) original image, (b) noisy image, (c) normal shrink applied image and (d) bilateral de-noising filter applied image.

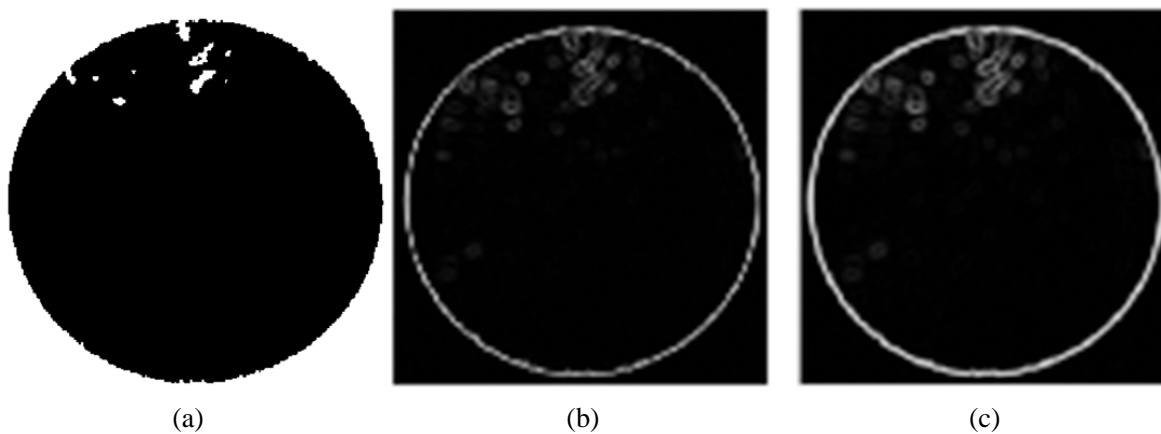


**Figure 7.** The segmented image using (a) Kirsch operator using a  $3 \times 3$  mask, (b) Sobel operator using a  $5 \times 5$  mask, and (c) using the OTSU segmentation.

optimal k-means [28] performed on the intensity histogram. The extension to multi-level thresholding was described in the original paper [27], and computationally efficient implementations have since been proposed [28].

After preparing the image for clustering purpose such that the healthy and unhealthy regions are distinguishable, K-Means algorithm was applied, which is a clustering algorithm with a fixed number of iterations and k value. The K-Means algorithm is based on an iterative framework, where in order to minimize the variation related to each cluster and to expand the variation between clusters the data components are replaced between clusters [29]. This clustering algorithm dedicates the pixel-based

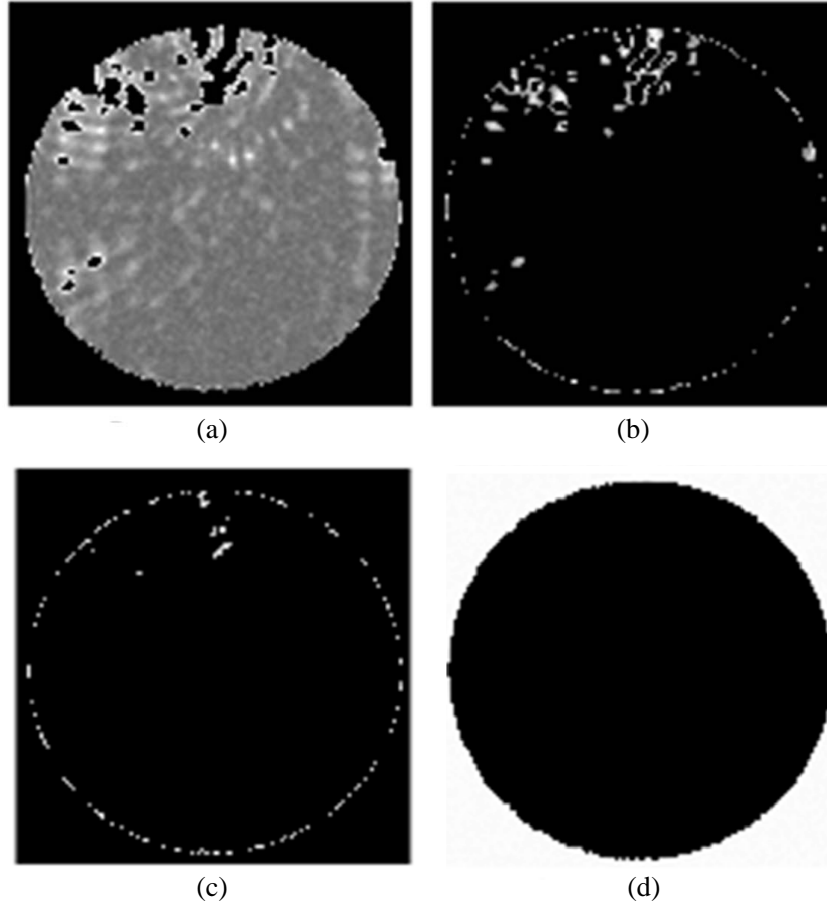


**Figure 8.** Clustered profiles while applying K-Means algorithm, (a) 1st cluster, (b) 2nd cluster, (c) 3rd cluster, and (d) 4th cluster.

segmentation of multi-band images. Each image stack is taken as a set of bands equivalent to the same image. Fig. 8 shows the clustered profiles of the reconstructed image while K-Means algorithm is applied. As shown in Fig. 8, for this study, the images consist of four bands, which are determined by different target value thresholds. The process will be terminated, when no elements are swapped over between clusters. In this study, the four K-Means algorithm clusters are considered based on four normalized thresholds values; 0.4, 0.6, 0.8, and 1. For presenting an image, each pixel is defined by an  $n$ -valued vector, where  $n$  indicates the number of bands. By having  $n$  vectors, each cluster is entitled using its centroid in an  $n$ -dimensional plane. The proposed K-Means algorithm procedure is executed as follows [30].

First, the  $K$  number of the initial cluster centers with random values are selected. Next, the samples,  $x$ , are distributed among the  $K$  clusters at the  $k$ th iterative step using the following relation:

$$\tau_i^{(t)} = \left\{ x_n : \left\| x_n - \mu_i^{(t)} \right\|^2 \leq \left\| x_n - \mu_j^{(t)} \right\|^2 \forall j, 1 \leq j \leq K \right\} \quad (4)$$

Then, new cluster centers  $\mu_i^{(k+1)}$ ,  $j = 1, 2, \dots, K$  can be calculated, by minimizing the sum of the squared distances from all points in  $\tau_i$  to the new cluster center. Here, the sample mean of  $\tau_i$  can minimize this set. Following, the new cluster center is considered in new iterative step:

$$\mu_i^{(t+1)} = \frac{1}{\left\| \tau_i^{(t)} \right\|} \sum_{x_p \in \tau_i^{(t)}} x_p \quad (5)$$

This step will be repeated until the assignments no longer change, i.e., when the algorithm has converged.

Finally, for clustering, Fuzzy C-Means (FCM) clustering algorithm is used. FCM permits every feature vector to belong to each cluster with a fuzzy truth-value. The FCM algorithm works to minimize the objective function, which is the generalization of the method of least squares

$$I_m = \sum_{i=1}^N \sum_{j=1}^c u_{ij}^m \|X_i - C_j\|^2 \quad 1 \leq m < \infty \quad (6)$$

In  $u_{ij}^m$ , the indexes  $i$  and  $j$  represent the object and its cluster membership value, respectively.  $1 \leq m < \infty$  is expressed as the fuzziness degree or fuzziness agent in fuzzy clustering algorithm.  $\|X_i - C_j\|^2$  represents the Euclidean distance between the object and cluster center. Clustering centers are calculated after the membership values are randomly assigned. Cluster centers are detected as below,

$$C_j = \left( \sum_{i=1}^N u_{ij}^m X_i \right) / \left( \sum_{i=1}^N u_{ij}^m \right) \quad (7)$$

The membership value in Eq. (7) is compared with the old value from the previous cycle. The process is repeated until the comparison value is less than the minimum value  $\varepsilon$  [30].

$$u_{ij} = \frac{1}{\sum_{k=1}^c \left( \frac{\|X_i - C_i\|}{\|X_i - C_k\|} \right)^{2/(m-1)}} \quad (8)$$

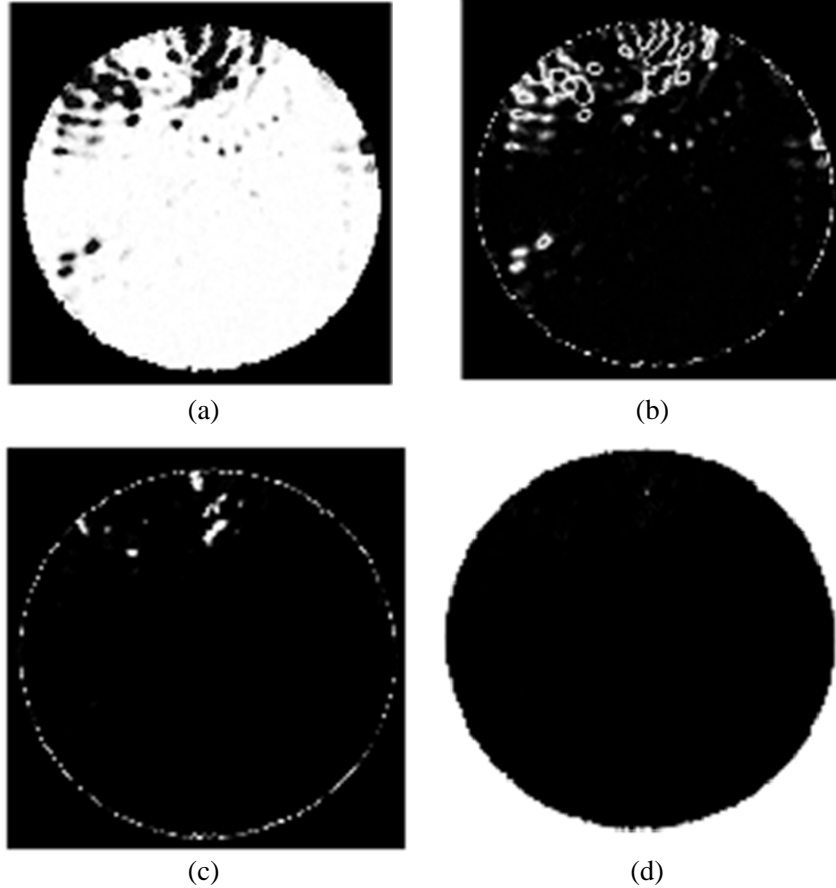


**Figure 9.** Clustering while applying FCM algorithm, (a) 1st cluster, (b) 2nd cluster, (c) 3rd cluster, and (d) 4th cluster.

The FCM clustering method specified briefly hereinabove has been utilized to separate the similarity image into two separate clusters in the presented study. The center average of two clusters gives the threshold value for edge detection, as shown in Fig. 9. Since the intensity of each pixel in the image confirms the amount of energy concentrated at each focal point, clustering is required to represent different amounts of this energy in each cluster. In other words, each cluster acts as an adaptive threshold. As shown in Fig. 9, four clusters with different energy intensities of the peaks are displayed. In the first case, there are large boundaries that represent the concentrated energy, while in the last cluster, due to the high threshold for filtering this concentrated energy, almost no purpose is revealed.

In order to demonstrate the classification performance, in Table 3 a comparison between the proposed method post-processing results and recently published similar papers in the literature is made. It can be seen that not only the accuracy of the proposed method is better than the other methods [11, 12] and [31], but also the extracted features and metrics show better results. It can therefore be concluded that the proposed MIS has a good capability for classification and segmentation of cerebrovascular targets. The algorithm was performed using Matlab R2019b tool in an Intel<sup>R</sup> Core<sup>TM</sup>i7 processor@ 3.60 GHz based Windows 10 Enterprise 64-bit operating system, and it has 7856 MB NVIDIA Graphics Processing Unit (GPU).

**Table 3.** Comparison of the proposed method to other published similar papers in the literature.

| Method              | Classification Accuracy | Time (second) | Processing unit   | SNR level       | Extracted Features numbers |
|---------------------|-------------------------|---------------|-------------------|-----------------|----------------------------|
| The proposed method | 97%                     | 13 s          | core i7 @ 1.8 GHz | 28 dB           | 12                         |
| Ref. [11]           | 96.1%                   | 31 s          | Not mentioned     | Noise less      | 3                          |
| Ref. [12]           | 93%                     | Not mentioned | core i7 @ 3.6 GHz | Noise-less      | 7                          |
| Ref. [31]           | 88%                     | 10 s          | core i7 @ 3.4 GHz | (45, 25, 10 dB) | 3                          |

#### 4. CONCLUSION

In this paper, first, a UWB-MIS is presented to detect and locate hemorrhage stroke in a multi-layer human head phantom using time-domain data. Then, the confocal method using DMAS beamforming is used for image reconstruction. Further, a novel post processing method including segmentation and K-Means and FCM based classification has been developed to distinguish between a healthy brain and a brain with hemorrhage stroke. The K-Means segmentation has been done based on the image pixel value characteristics. The FCM algorithm can efficiently separate the similarity image into two separate clusters from the reconstructed image. The results show that the developed imaging system has a good ability in detecting even small hemorrhage stroke targets with radius of 1 cm in a biological medium. It can be seen from Table 3 that not only the accuracy of the proposed method is better than that for recently reported methods [11, 12, 26], but also the extracted features and metrics have better results. Therefore, the proposed MIS has a good capability of classifying and segmenting cerebrovascular targets.

#### REFERENCES

- Scapaticci, R., J. Tobon, G. Bellizzi, F. Vipiana, and L. Crocco, "Design and numerical characterization of a low-complexity microwave device for brain stroke monitoring," *IEEE Transactions on Antennas and Propagation*, Vol. 66, No. 12, 7328–7338, Dec. 2018.
- Sohani, B., G. Tiberi, N. Ghavami, M. Ghavami, S. Dudley, and A. Rahimi, "Microwave imaging for stroke detection: Validation on head-mimicking phantom," *2019 Photonics & Electromagnetics Research Symposium — Spring (PIERS — SPRING)*, 940–948, Rome, Italy, Jun. 17–20, 2019.

3. Wang, J., X. Jiang, L. Peng, X. Li, H. An, and B. Wen, "Detection of neural activity of brain functional site based on microwave scattering principle," *IEEE Access*, Vol. 7, 13468–13475, 2019.
4. Ilja, M., A. Massa, D. Vrba, O. Fiser, M. Salucci, and J. Vrba, "Microwave tomography system for methodical testing of human brain stroke detection approaches," *International Journal of Antennas and Propagation*, 2019.
5. Santorelli, A., E. Porter, E. Kirshin, Y. J. Liu, and M. Popovic, "Investigation of classifiers for tumor detection with an experimental time domain breast screening system," *Progress In Electromagnetics Research*, Vol. 144, 45–57, 2014.
6. Pokorny, T. and J. Tesarik, "Microwave stroke detection and classification using different methods from MATLAB's classification learner toolbox," *2019 European Microwave Conference in Central Europe (EuMCE)*, 500–503, IEEE, 2019.
7. Conceicao, R. C., M. O'Halloran, M. Glavin, and E. Jones, "Support vector machines for the classification of early-stage breast cancer based on radar target signatures," *Progress In Electromagnetics Research B*, Vol. 23, 311–327, 2010.
8. Rahama, Y. A., O. A. Aryani, U. A. Din, M. A. Awar, A. Zakaria, and N. Qaddoumi, "Novel microwave tomography system using a phased-array antenna," *IEEE Trans. Microw. Theory Tech.*, Vol. 66, 5119–5128, 2018.
9. Franceschini, S., M. Ambrosanio, F. Baselice, and V. Pascazio, "Neural networks for inverse problems: The microwave imaging case," *2021 15th European Conference on Antennas and Propagation (EuCAP)*, 1–5, IEEE, Mar. 2021.
10. Bevacqua, M. T., S. Di Meo, L. Crocco, T. Isernia, G. Matrone, and M. Pasian, "A quantitative approach for millimeter-wave breast cancer imaging," *2021 15th European Conference on Antennas and Propagation (EuCAP)*, 1–3, IEEE, Mar. 2021.
11. Chaplot, S., L. M. Patnaik, and N. R. Jagannathan, "Classification of magnetic resonance brain images using wavelets as input to support vector machine and neural network," *Biomedical Signal Processing and Control*, Vol. 1, No. 1, 86–92, 2006.
12. Rana, S. P., M. Dey, G. Tiberi, L. Sani, A. Vispa, G. Raspa, M. Duranti, M. Ghavami, and S. Dudley, "Machine learning approaches for automated lesion detection in microwave breast imaging clinical data," *Sci. Rep.*, Vol. 9, 1–12, 2019.
13. Dachena, C., A. Fedeli, A. Fantì, M. B. Lodi, M. Pastorino, and A. Randazzo, "A microwave imaging technique for neck diseases monitoring," *2021 15th European Conference on Antennas and Propagation (EuCAP)*, 1–5, IEEE, Mar. 2021.
14. Ojaroudi, M., S. Bila, and M. Salimitorkamani, "A novel machine learning approach of hemorrhage stroke detection in differential microwave head imaging system," *2020 European Conference on Antennas and Propagation*, 2020.
15. Nanni, L., S. Ghidoni, and S. Brahmam, "Handcrafted vs. non-handcrafted features for computer vision classification," *Pattern Recognition*, Vol. 71, 158–172, 2017, ISSN 0031-3203.
16. CST Microwave Studio. ver. 2016, CST, Framingham, MA, USA, 2016.
17. Li, X., M. Jalilvand, Y. L. Sit, and T. Zwick, "A compact double-layer on-body matched bowtie antenna for medical diagnosis," *IEEE Transactions on Antennas and Propagation*, Vol. 62, No. 4, 1808–1816, 2014.
18. Jalilvand, M., X. Li, J. Kowalewski, and T. Zwick, "Broadband miniaturised bow-tie antenna for 3D microwave tomography," *Electronics Letters*, Vol. 50, No. 4, 244–246, 2014.
19. Jamlos, M. A., W. A. Mustafa, N. Husna, S. Z. Syed Idrus, W. Khairunizam, I. Zunaidi, Z. M. Razlan, and A. B. Shahriman, "Ultra-wideband confocal microwave imaging for brain tumor detection," *IOP Conference Series: Materials Science and Engineering*, Vol. 557, No. 1, 012002, IOP Publishing, 2019.
20. Chandra, R., H. Zhou, I. Balasingham, and R. M. Narayanan, "On the opportunities and challenges in microwave medical sensing and imaging," *IEEE Transactions on Biomedical Engineering*, Vol. 62, No. 7, 1667–1682, 2015.

21. Benny, R., T. A. Anjit, and P. Mythili, "An overview of microwave imaging for breast tumor detection," *Progress In Electromagnetics Research B*, Vol. 87, 61–91, 2020.
22. Ahsan, S., M. Koutsoupidou, E. Razzicchia, I. Sotiriou, and P. Kosmas, "Advances towards the development of a brain microwave imaging scanner," *2019 13th European Conference on Antennas and Propagation (EuCAP)*, 1–4, IEEE, Mar. 2019.
23. Fhager, A., S. Candefjord, M. Elam, and M. Persson, "3D simulations of intracerebral hemorrhage detection using broadband microwave technology," *Sensors*, Vol. 19, No. 16, 3482, 2019.
24. Wu, Y., B. Liu, and M. Zhu, "A single-pair antenna microwave medical detection system based on unsupervised feature learning," *International Conference on Computational Social Networks*, 404–414, Springer, Dec. 2018.
25. Zhang, Y.-D. and L. Wu, "An MR brain images classifier via principal component analysis and kernel support vector machine," *Progress In Electromagnetics Research*, Vol. 130, 369–388, 2012.
26. Parvati, K., P. Rao, and M. Mariya Das, "Image segmentation using gray-scale morphology and marker-controlled watershed transformation," *Discrete Dynamics in Nature and Society*, Vol. 2008, 2008.
27. Otsu, N., "A threshold selection method from gray-level histograms," *IEEE Trans. Sys. Man. Cyber.*, Vol. 9, No. 1, 62–66, 1979, doi: 10.1109/TSMC.1979.4310076.
28. Liu, D., "Otsu method and K-means," *Ninth International Conference on Hybrid Intelligent Systems*, Vol. 1, 344–349, IEEE, 2009.
29. Vijayabhanu, R. and V. Radha, "Recognition and elimination of missing values and outliers from an anaerobic wastewater treatment system using K-Means cluster," *2010 3rd International Conference on Advanced Computer Theory and Engineering (ICACTE)*, Vol. 4, V4-186, 2010.
30. Tripathi, S., R. S. Anand, and E. Fernandez, "A review of brain MR image segmentation techniques," *Proceedings of International Conference on Recent Innovations in Applied Science, Engineering & Technology*, 16–17, 2018.
31. Guo, L. and A. Abbosh, "Stroke localization and classification using microwave tomography with k-means clustering and support vector machine," *Bioelectromagnetics*, Vol. 39, No. 4, 312–324, May 2018, doi: 10.1002/bem.22118.Epub2018Mar25. PMID: 29575011.